ACS NANO
Cite This: ACS Nano 2019, 13, 8023−8034
www.acsnano.org

ARTICLE

Supervised Learning and Mass Spectrometry Predicts the *in Vivo* Fate of Nanomaterials

James Lazarovits,[†,‡,▽] Shrey Sindhwani,[†,‡,▽] Anthony J. Tavares,[†,‡,▽] Yuwei Zhang,[†,‡] Fayi Song,[†,‡] Julie Audet,[†,§] Jonathan R. Krieger,[∥] Abdullah Muhammad Syed,[†,‡] Benjamin Stordy,[†,‡] and Warren C. W. Chan*[,†,‡,§,⊥,#]

[†]Institute of Biomaterials and Biomedical Engineering, University of Toronto, 164 College Street, Toronto, Ontario M5S 3G9, Canada

[‡]Terrence Donnelly Centre for Cellular and Biomolecular Research, University of Toronto, 160 College Street, Toronto, Ontario M5S 3E1, Canada

[§]Department of Chemical Engineering, University of Toronto, 200 College Street, Toronto, Ontario M5S 3E5, Canada

[∥]SPARC BioCentre, The Hospital for Sick Children, The Peter Gilgan Centre for Research & Learning, 686 Bay Street, 21st Floor Toronto, Ontario M5G 0A4, Canada

[⊥]Department of Chemistry, University of Toronto, 80 St. George Street, Toronto, Ontario M5S 3H6, Canada

[#]Department of Materials Science and Engineering, University of Toronto, 184 College Street, Toronto, Ontario M5S 3E1, Canada

Supporting Information

ABSTRACT: **The surface of nanoparticles changes immediately after intravenous injection because blood proteins adsorb on the surface. How this interface changes during circulation and its impact on nanoparticle distribution within the body is not understood. Here, we developed a workflow to show that the evolution of proteins on nanoparticle surfaces predicts the biological fate of nanoparticles *in vivo*. This workflow involves extracting nanoparticles at multiple time points from circulation, isolating the proteins off the surface and performing proteomic mass spectrometry. The mass spectrometry protein library served as inputs, while blood clearance and organ accumulation were used as outputs to train a supervised deep neural network that predicts nanoparticle biological fate. In a double-blinded study, we tested the network by predicting nanoparticle spleen and liver accumulation with upward of 94% accuracy. Our neural network discovered that the mechanism of liver and spleen uptake is due to patterns of a multitude of nanoparticle surface adsorbed proteins. There are too many combinations to change these proteins manually using chemical or biological inhibitors to alter clearance. Therefore, we developed a technique that uses the host to act as a bioreactor to prepare nanoparticles with predictable clearance patterns that reduce liver and spleen uptake by 50% and 70%, respectively. These techniques provide opportunities to both predict nanoparticle behavior and also to engineer surface chemistries that are specifically designed by the body.**

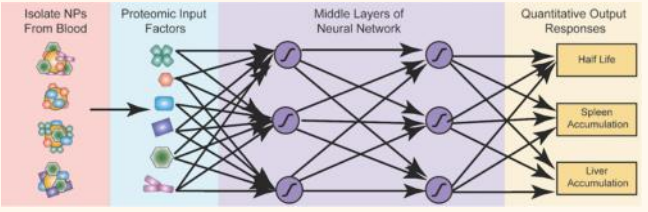

KEYWORDS: *nanoparticles, protein corona, mass spectrometry, neural networks, machine learning, artificial intelligence, predictive biology*

Despite having exquisite control over nanoparticle design, controlling nanoparticle fate *in vivo* remains a major barrier to clinical translation. This is because the chemical and physical properties of nanoparticles are immediately altered as they interface with the blood following intravenous administration.[1−8] These alterations continue as nanoparticles interact with the various biological components of cells, tissues, and organs. The combination of these alterations and interactions augment the fate of nanoparticles inside of the body, resulting in minimal accumulation at the target site and subsequent off-target toxicity *in vivo*.[1,2] Consequently, many engineered nanoparticles have not been translated to the clinic because these uncontrollable interactions dictate nanoparticle biodistribution and act as biological barriers to nanomedicine.[2−4] A first step toward improving translation is to identify the relationship between the biological barriers that nanoparticles face and their biological fate. It has been suggested that the hundreds of blood proteins that adsorb to the nanoparticle surface upon administration and during circulation might be the key link

Received: April 10, 2019
Accepted: June 21, 2019
Published: June 21, 2019

DOI: 10.1021/acsnano.9b02774
ACS Nano 2019, 13, 8023−8034

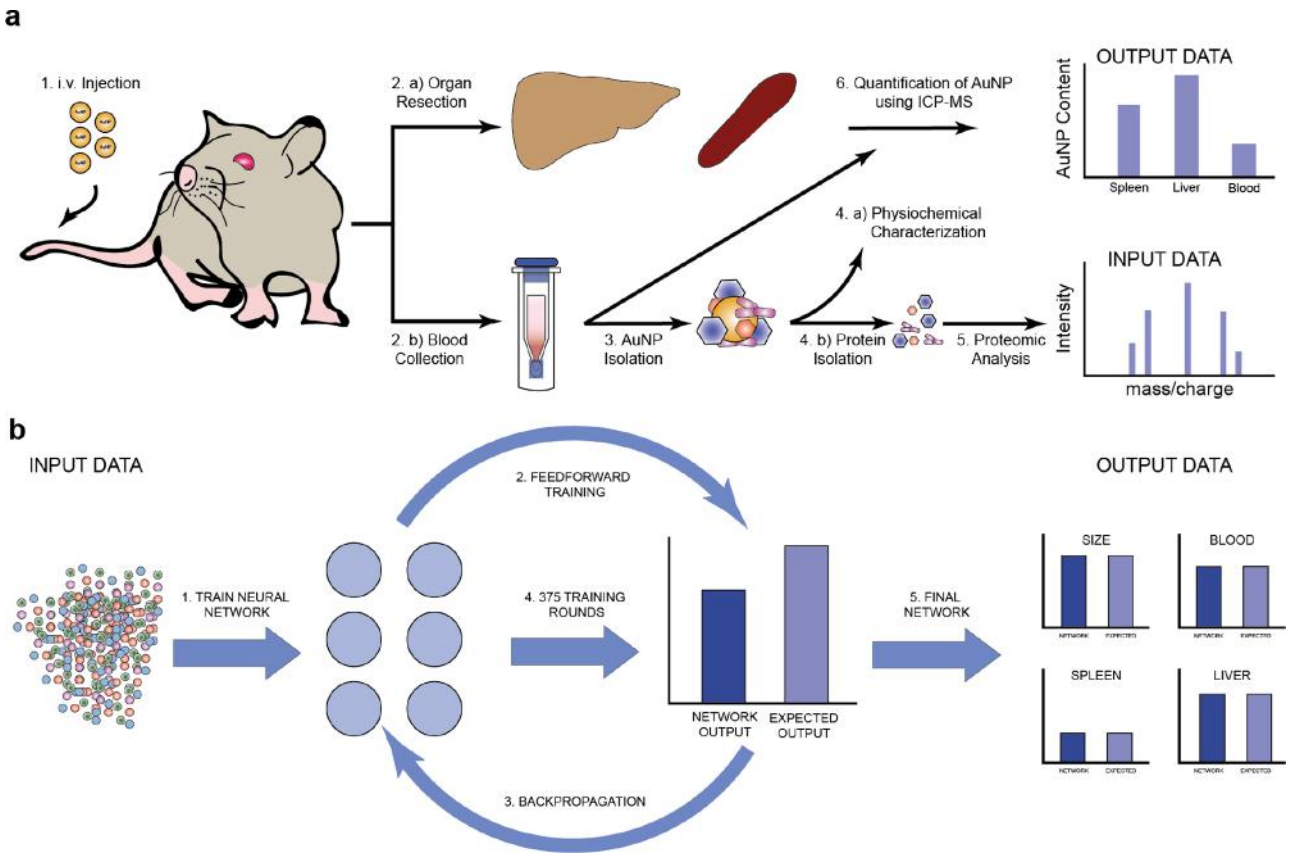

Figure 1. Methodology for building and training the predictive neural network. (A) PEGylated AuNPs were injected intravenously into rats, and blood was sampled at multiple times over 24 hours from the same animal. AuNPs suspended in serum were separated using centrifugation and underwent physiochemical characterization. Proteins were stripped off and digested for LC−MS/MS processing and analysis. This proteomic analysis formed the input for the neural network (NN). On the other hand, liver and spleen were also resected from rats and digested to measure AuNP organ accumulation using ICP−MS. The organ accumulation of AuNPs and the size of the nanoparticle formed the output of our NN. (b) NN inputs the protein data and iterates it through a feedforward and backpropagation cycle to build a mathematical model for predicting the output parameters.

between these barriers and nanoparticle biological fate. While several studies have characterized the composition of the adsorbed protein population,[3−12] the link between protein composition and nanoparticle biological fate inside of the body has not been established. Previous studies have tried to assess these relationships using one-protein-at-a-time knockout models and have shown that no single protein is solely responsible for clearance.[3] Rather than just one protein, it may be the combination of proteins specific to the nanoparticle that dictate biological fate.[1,13,14] The specific influence of each individual surface-adsorbed protein let alone interrogating combinations of them is technically challenging and laborious to determine *in vivo*. Therefore, to determine how these combinations of proteins influence biological behavior, we needed a technique to resolve the multivariate and multifactorial changes that occur on the nanoparticles' surface as they circulate in the blood. We hypothesized supervised learning was the most appropriate method to resolve these patterns, because they are built to map relationships between input and output data without explicitly being programmed.[15−17]

RESULTS AND DISCUSSION

Previous studies have used the *in silico* methods of hierarchical clustering (HCA) and principle component analysis (PCA) to develop predictive relationships between protein adsorption and *in vitro* cell uptake.[3−12] However, these statistical techniques cannot predict nanoparticle *in vivo* fate using surface adsorbed proteins.[10] The main reason is the complexity of *in vivo* transport of nanoparticles. During transit, they interact with more biological components and organs and therefore have many more variables than *in vitro*.[10] From a modeling perspective, HCA and PCA are not effective at handling high dimensionality data and where data points do not have very large variations and differences. To solve this problem, we used supervised learning to predict the fate of nanoparticles *in vivo* as it is better at resolving relationships in high dimensionality data. Neural networks do this by creating multiple intermediary transformation layers that calculate both the linear and nonlinear relationships between inputs and outputs. Even if the data exhibits small variation, the network exposes these subtle differences by backpropagating prediction error between inputs and outputs until the test error reaches a minimum. This systematic approach to analyze multiparametric data without knowledge of the relationships between inputs and outputs enabled us to map relationships in high dimensionality data sets that have subtle differences in an unbiased manner. To build the network, we first constructed our training data set that contained proteomic data from circulating nanoparticles for inputs and quantitative biodistribution using elemental analysis as the outputs.

DOI: 10.1021/acsnano.9b02774
ACS Nano 2019, 13, 8023−8034

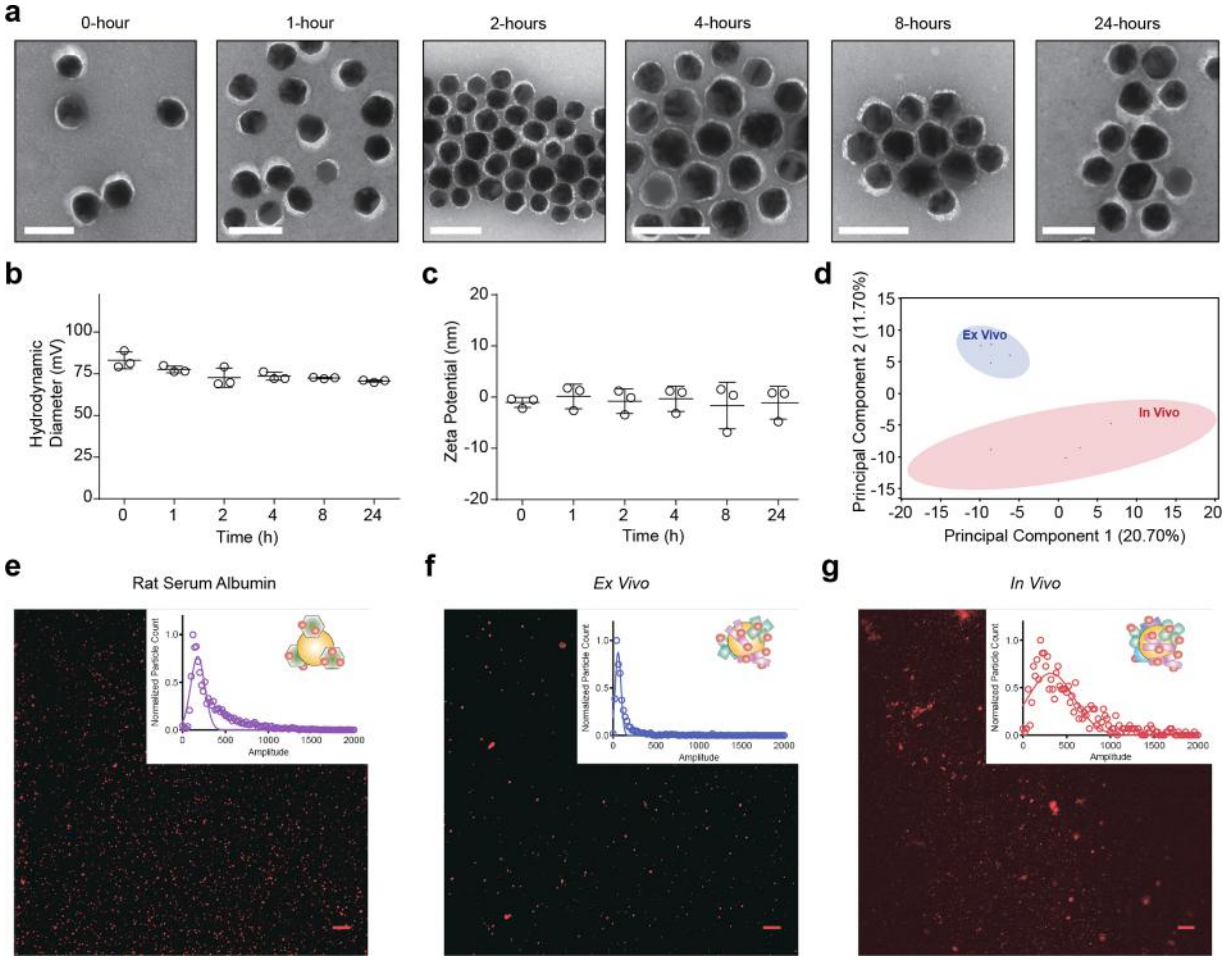

Figure 2. Characterization of circulating AuNPs. (a) Morphology of AuNPs visualized by TEM show a layer of surface adsorbed proteins around the nanoparticles that is less electron-dense. Other physiochemical properties such as (b) hydrodynamic size and (c) zeta potential do not change over 24 hours. (d) PCA plots of proteins on the surface of AuNPs show that there is variability in the types of proteins that adsorb and exchange on the nanoparticle surface during circulation ($p < 0.01$, $F = 3.37$). This variability is greater *in vivo* when compared to incubating AuNPs in *ex vivo* serum (e–g). Single-molecule fluorescence microscopy of individual nanoparticles also revealed greater heterogeneity at a single nanoparticle level for (g) *in vivo* AuNPs when compared nanoparticles coated with (f) *ex vivo* blood or with only (e) rat serum albumin. ($p < 0.0001$, $F = 63.90$). The scale bar represents 10 μm. p-Values were obtained from an unpaired t test and two-tailed F-test and one-way ANOVA for PCA and the single molecule analysis, respectively.

We first developed methods to extract engineered nanoparticles from blood circulation at multiple time points and then isolated the surface-adsorbed proteins.[1,7] We collected multiple time points instead of single end points in order to sample a detailed profile of interactions between blood proteins and the nanoparticle surface. We selected Sprague–Dawley rats as our model animal to enable extraction of sufficient quantities of nanoparticles at each time point. We did not use mice for these studies because they do not have enough blood for isolating nanoparticles from the same animal over multiple time-points for temporal analysis. We used gold nanoparticles (AuNP) as our model nanomaterial because they are readily synthesized with control over size and surface chemistry and can be elementally quantified using inductively coupled plasma-mass spectrometry (ICP–MS).[13,14,18] We selected ICP–MS as a means to collect output data because it provides direct quantification of metallic nanoparticles and is widely used in the literature. In comparison, the purpose of the network is to gather proteomic insights from the surface of circulating nanoparticles. To ensure our AuNP did not aggregate in the blood and had long blood half-lives for higher yield in isolation and analysis,[19−21] we saturated the AuNP surface with polyethylene glycol (PEG) at 5 PEG/nm^2 (Figure S1).[22] Following PEGylation, we then injected the AuNPs into rats. Blood was extracted at 1, 2, 4, 8, and 24 hours post administration (Figure 1).[14,18] We separated the cellular and acellular blood components and then isolated the AuNP from serum using centrifugation. The physicochemical properties (size, surface charge, morphology) of the extracted AuNPs were measured, and the proteins on the AuNP surface were extracted and processed for proteomic analysis using liquid chromatography tandem mass spectrometry (LC–MS/MS).[1] The proteins' label-free quantitative (LFQ) intensities were used as the inputs for the model. To build the output data, we used ICP–MS to quantify gold in the blood over 24 hours, and the gold content in the spleen and the liver at the end-point (Figure 1a). Together, this workflow enabled us to train the neural network using proteins LFQ intensities as inputs and nanoparticle biological fate as outputs (Figure 1b). Before we trained the network, we first verified that extracted AuNP remained monodisperse throughout circulation.

DOI: 10.1021/acsnano.9b02774
ACS Nano 2019, 13, 8023–8034

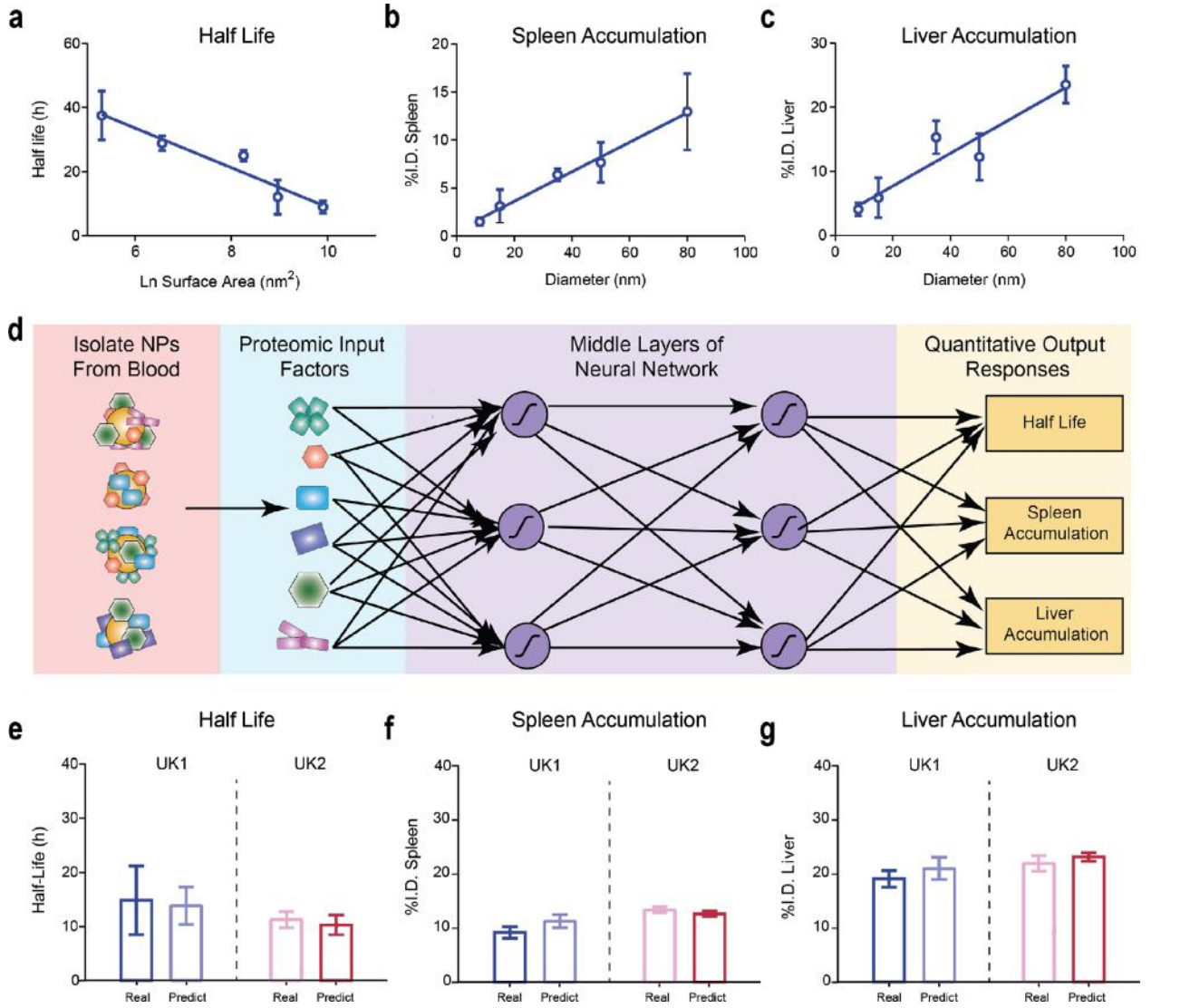

Figure 3. Neural network trained on proteomic information from five sizes of circulating gold nanoparticles predicts biological behavior. We quantified the (a) half-life, (b) spleen accumulation, and (c) liver accumulation of the five gold nanoparticles using inductively coupled plasma mass spectrometry. These values were used as quantitative outputs for the network. (d) Proteins isolated from the surface of 8, 15, 35, 50, and 80 nm gold nanoparticles over five time points in circulation were used as inputs for the neural network. After training and validation, the network was able to predict the biological behavior of two unknown (UK) nanoparticles, termed UK1 and UK2 with (e) 84.78% and 91.00% accuracy for half-life, (f) 77.32% and 92.69% for spleen accumulation, and (g) 81.02% and 93.98% for liver accumulation. Building and training the network was performed using JMP Pro statistical discovery software (V12.2.0) from SAS Institute, Inc. n = 3. Error bars denote the standard deviation.

To ensure that compositional differences within the adsorbed protein population were not due to a change in the stability of AuNP physicochemical properties, we measured them before injection and during circulation in the blood. Although PEGylated AuNP should remain stable in circulation, we wanted to verify this because aggregation influences protein binding[23,24] and organ accumulation. This would influence both the inputs and outputs used to build the neural network. Following administration and the initial protein adsorption events, AuNP increased in hydrodynamic size and stabilized in surface charge density (Figure 2a) in accordance with previously relevant literature (Figure S2).[1,4,6,7] While the physicochemical properties did not change with time following the initial adsorption event, surface proteins varied (Figure S3). Because traditional spectral count thresholding biases the data to larger proteins, we used extracted MS1 (first stage of mass spectrometry detection) ion currents to measure LFQ intensities using Peaks Studio.[25−27] Unsupervised hierarchical clustering revealed a change in protein abundances over time as well as the relative differences and variability between *in vivo* and *ex vivo* incubation methods. To show these differences more explicitly, we used the LFQ intensities at each time point as inputs for a principal component analysis (PCA). In PCA, the first principal component explains the most variation, and this was 12.13% *in vivo* compared to 0.16% *ex vivo* (Figure 2b) (P < 0.01, F = 3.37). When compared to nanoparticles incubated with blood *ex vivo*, the *in vivo* workflow captured a much broader protein profile and a greater variability from one time point to another for the same sample. This broad protein profile came from differences across time points and not from the variability among animals because the proteins between animals for the same time point were not significantly different

DOI: 10.1021/acsnano.9b02774
ACS Nano 2019, 13, 8023−8034

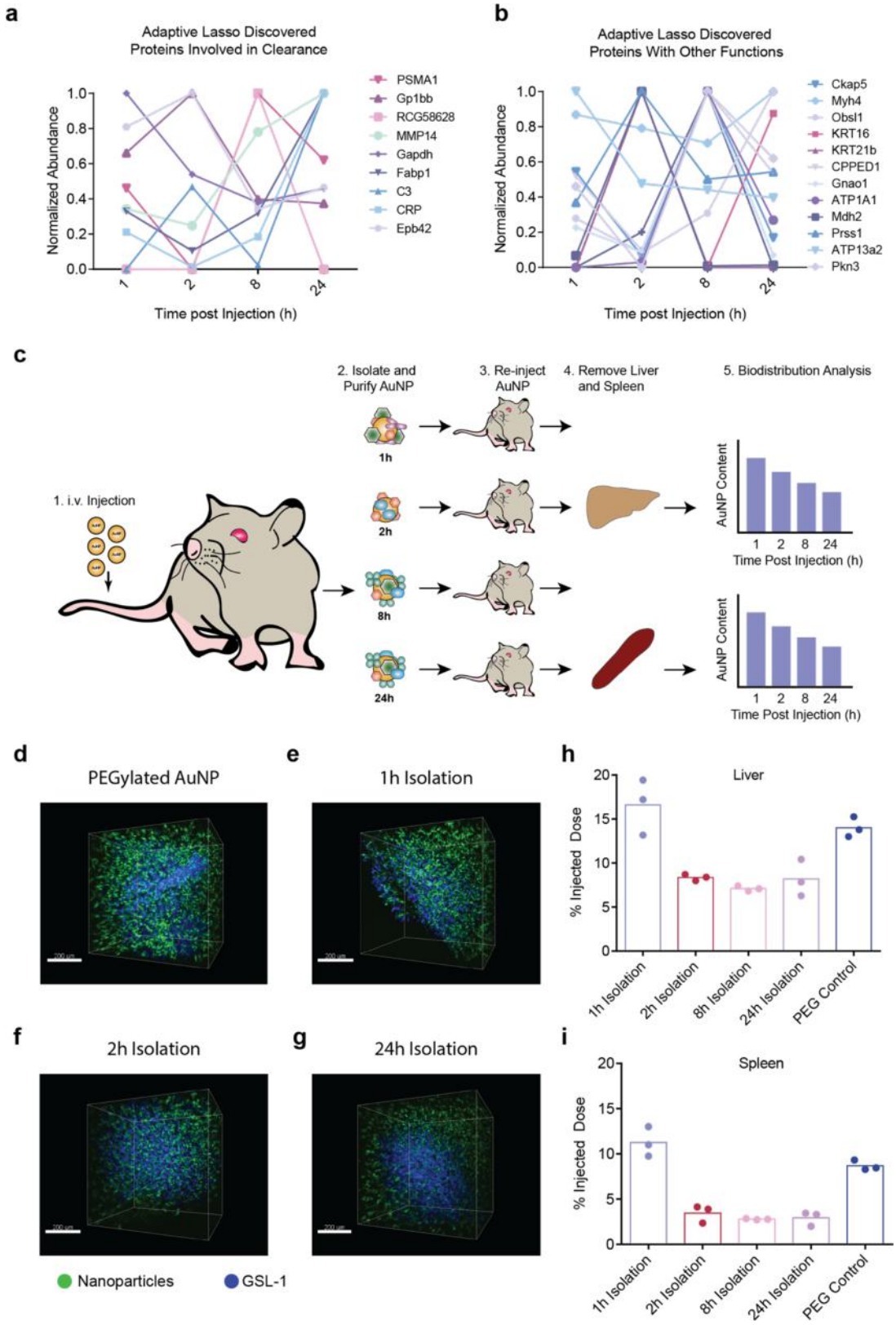

Figure 4. Serial injection of nanomaterials for biodistribution analysis shows combinations of proteins on surface dictates clearance into liver and spleen. Proteins were separated based on their function determined through the Universal Protein Databank. Neither (a) clearance related nor (b) other functional proteins exhibited any clear trend as they increased and decreased in abundance over time. (c) In Serial Injection of Materials for Biodistribution Analysis (SIMBA), nanoparticles were injected into a rat and removed from circulation at 1, 2, 8, and 24 hours post injection, the nanoparticles were extracted at each time point and then administered into four other rats, and their biodistribution was measured after 24 hours. We first used 3D imaging to determine the difference in distribution of nanoparticles at early versus late time points. (d) PEGylated nanoparticle control of (e) 1 hour nanoparticle, (f) 2 hours nanoparticle, and (g) 24 hours nanoparticle. Nanoparticles are fluorescently visualized in green, GSL1 lectin (blood vessel staining) in blue. We confirmed these differences

DOI: 10.1021/acsnano.9b02774
ACS Nano 2019, 13, 8023−8034

Figure 4. continued

using inductively couple plasma-mass spectrometry (ICP−MS) and found that 1 and control particles were nonsignificantly different. 2, 8 and 24 hours were significantly different in both the (h) liver ($P < 0.0223$) and (i) spleen ($P < 0.0036$). *In vivo* studies were $n = 3$ per condition. Statistical significance was determined using one-way ANOVA with Tukey correction for multiple comparisons.

($P < 0.0001$, $F = 15.44$). To further highlight the differences in heterogeneity, we took the protein-nanoparticle isolates from rats, AuNP incubated with serum *ex vivo*, and a control solely comprised of the protein rat serum albumin. The surface adsorbed proteins of all three nanoparticle samples were labeled with fluorescent dye (Alexa-647). We then used single molecule fluorescence microscopy to analyze the fluorescence modes of the nanoparticle samples, as this enabled spatial resolution of individual nanoparticles within each ensemble (Figure S4). Using the fluorescence amplitude as an indirect method to quantify protein heterogeneity, we found that inter-nanoparticle variability was much higher *in vivo* (Variance: 82.69%) when compared to labeled albumin (Variance: 46.64%) and *ex vivo* serum (Variance: 57.13%) (Figure 2e−g) ($P < 0.0001$, $F = 63.90$). Overall, we found that as nanoparticles circulate in the blood, their physical−chemical properties change over time. This physio-chemical interrogation also guided us to design parameters such as nanoparticle size, circulation time points for the training, and validating the neural network built. The input data set could capture the heterogeneous changes occurring on nanoparticle surface during circulation. These heterogeneous interactions are present not only at the population level, but also for single nanoparticles. Since we sampled at many time points, it was possible to capture the distribution of protein−nanoparticle interactions in circulation. By feeding this proteomic data into the neural network and providing nanoparticle organ accumulation and half-life as output, we could build a model to map the relationship between inputs and outputs without the need for specific programming.

To train the neural network, we first assembled a training data set. We used five different AuNP core sizes (8, 15, 35, 50, and 80 nm), each functionalized with a consistent surface 5 PEG/nm^2 density (Figure 3a) (Supplementary Tables S1 and S2). Changing AuNP size induces large changes in blood half-life and spleen and liver uptake. Therefore, we constrained our prediction variables to how size-dependent protein-adsorption patterns influences large changes in biological behavior.[1,7,13,28] We validated that increasing nanoparticle size changed protein abundances ($P < 0.0001$, $F = 9.121$), increased the blood clearance rate, and increased spleen and liver uptake (Figures 3b−d and S5). Based on all time points, nanoparticle sizes, 707 proteins detected from LC-MS, and biological replicates (Supplementary Table S2), we had a total of 63, 630 protein LFQ intensities for the input data set. Nanoparticle blood half-life, spleen and liver accumulation, and diameter obtained from dynamic light scattering were the outputs. Previous studies have been unable to correlate protein inputs to biological behavior through commonly used techniques.[10] So, we used a network that contained three nodes and two layers per node that mapped the relationships through both nonlinear and linear hyperbolic tangent activation functions (see methods). The network cycled through 375 iterations of feedforward and backpropagation learning, was regularized using K-fold cross validation, and avoided overfitting *via* an early stopping rule (See Table S3 for performance, methods for detailed setup parameters and our Python code).[15,29] Once successfully trained, we performed a double-blind study to validate its accuracy and ensure we did not overfit the model.

We next tested the neural network's prediction accuracy. We challenged the model to predict the half-life, spleen and liver accumulation, and diameter of AuNPs of unknown (UK) diameter but identical surface chemistry. The individuals performing the experiment and analyzing the data were unaware to the physicochemical properties of two test nanoparticle formulations, termed UK1 and UK2 (Figure S6). UK1 and UK2 contained 21 210 input proteomic data points, and these values were not used in the training of the model itself. The prediction accuracy was determined by comparing all the values predicted by the neural network against the experimental size, half-life and spleen and liver accumulation from ICP−MS and DLS. The model predicted the biological fate of nanoparticles with 77.32−93.98% accuracy (Figure 3e−g). Specifically, when compared to the measured ICP−MS values across all replicates, the neural network was 84.78% and 91.00% accurate for blood half-life, 77.32% and 92.69% accurate for spleen accumulation, and 81.02% and 93.98% accurate for liver accumulation, for UK1 and UK2, respectively (Table S4). The neural network could also predict the size of the nanoparticle that was injected with 99% (UK1) and 90% accuracy (UK2) (Figure S7). We verified that five time points provided the highest prediction accuracy and tested different aspects of tuning model performance in Supplementary Section S8. It should be noted that nanoparticles of a particular size are an ensemble of different sizes of a Gaussian distribution centered at that size as mean. The reported size is the mean of the distributions. This means that as sizes get closer to each other, their protein profiles might share some common proteins and their biodistributions will not be statistically different. For greater accuracy in training and prediction, one would require sub nm standard deviation in particle synthesis which in current bulk synthesis scheme is difficult. Nonetheless, These results reflect the importance of profiling protein adsorption on nanoparticle surfaces over multiple time points in order to build a model that accurately predicts biological fate. To ensure these techniques were generalizable, we built a neural network that predicted biological fate of polymeric nanoparticles (Figure S9 and Table S5).[30] These results indicate that proteins, irrespective of nanoparticle composite material, govern nanoparticle biological behavior. And it is the combinations of these hundreds of surface-adsorbed proteins that evolve during circulation in the blood that constitute the link between biological barriers and nanoparticle biological fate.

Based on our network analysis, we discovered that the mechanism of nanoparticle clearance depends on combinations of proteins and not a single protein. This is because recent studies implicated single proteins in mediating clearance (e.g., Stab2, Clusterin, CD47).[31−33] The fact that a multitude of proteins that adsorb on the nanoparticle surface drive uptake in the liver and spleen suggests that it would be difficult to manipulate single cell receptors or surface adsorbed proteins toward changing the overall distribution patterns of therapeutic nanomaterials. In an effort to learn which proteins were most

DOI: 10.1021/acsnano.9b02774
ACS Nano 2019, 13, 8023−8034

important for this uptake, we ran an adaptive lasso and identified a subset of 21 proteins that were most associated with biodistribution (Figures 4a,b and S10).[34,35] It was interesting to discover that these 21 proteins could predict spleen and liver uptake with comparable accuracy when compared to the neural network prediction based on 707 proteins (Figure S11). If linear relationships were obvious, it may suggest that as the number of proteins increase liver and spleen uptake would increase. But these proteins did not increase or decrease collectively over time, but rather the adsorption pattern varied at different rates (Figure 4a and b). This suggested to us that clearance is dictated by combinations of proteins that form patterns on the nanoparticle surface. These combinations indicate to the body whether or not that nanoparticle should be cleared.

A traditional strategy to test this mechanism is systematically varying proteins and/or knocking out the receptors. However, since multiple proteins are involved, it is difficult to inhibit them using chemical or biological means. It would also be extremely difficult for traditional biological experiments to knockout 21, let alone 707 proteins, and then test the impact of combinations of protein patterns on nanoparticle biodistribution. Therefore, to prove that protein patterns control nanoparticle accumulation, we developed a technique termed Serial Injection of Materials for Biodistribution Analysis (SIMBA). In SIMBA, we injected nanoparticles into a rat (referred to as donor rat), removed them from circulation at different time points (1, 2, 8, and 24 hours) post injection, extracted the nanoparticles at each time point, then administered them into a different rat (referred as the acceptor rat) and measured their biodistribution after 24 hours (Figure 4c). SIMBA allowed us to capture different snapshots of protein evolution on the nanoparticle surface by isolating nanoparticles at different time points in circulation. Since rapid clearance is observed within the first few hours, we expected that nanoparticles isolated at early time points would accumulate more into the liver and spleen in comparison to those isolated at later time points. We used 3D imaging, ultrastructural transmission electron microscopy, and ICP−MS to confirm this hypothesis. Qualitatively, we observed that nanoparticles isolated at 1 hour postinjection from a donor rat behaved the same as those that had not been exposed to the animal. Nanoparticles isolated at 2 hours from the donor rat exhibited very different uptake and distribution patterns inside of the liver of the acceptor rat compared to those isolated at 1 hour (Figure 4d−g, Figure S12, and Table S6). We then examined the quantitative differences in whole-liver and spleen uptake using ICP−MS. Quantitatively, nanoparticles isolated at 1 hour postinjection exhibited the exact same liver and spleen uptake as nanoparticles that had not been prior exposed to the body. However, nanoparticles isolated at 2, 8, and 24 hours had on average 70% less spleen and 50% less liver uptake (Figure 4h,i). Specifically, donor rats from 1 hour and PEG control had an average liver and spleen uptake of 15.31 ± 2.34 and 9.97 ± 1.62% injected dose, whereas the 2, 8 and 24 hours had an average % injected dose of 7.88 ± 1.51 and 3.06 ± 0.66 for liver and spleen, respectively. Our results from the neural network analysis and SIMBA confirm that protein patterns, and not individual proteins, dictate nanoparticle removal from circulation. This suggests that the body modifies the chemical properties of the nanoparticle, and those with longer circulation are not cleared because they lack the pattern of combinations of proteins appropriate for liver and spleen uptake. These combinations of proteins cannot be recapitulated artificially. So SIMBA enables us to both evaluate this mechanism and use the body as a bioreactor to controllably build surface chemistries that avoid liver and spleen uptake.

CONCLUSIONS AND FUTURE OUTLOOK

We provide a detailed analysis of the nanoparticle surface chemistry as they circulate in the animal. The evolution of this chemistry appears to dictate their interactions with cells and tissues in the body. Using supervised learning, we can process these interactions to predict the clearance and biodistribution of engineered nanomaterials *in vivo*. We must continue to feed more data into this learning system and build more sophisticated neural networks with greater predictive power. Artificial learning systems should be a key component in the future design of therapeutic and diagnostic agents as these systems would reduce the total number of animals and material formulations required for preclinical studies. Our work creates an avenue for the convergence of deep neural networks and mass spectrometry to guide the design implementation of administered therapeutics with strategies to synthesize nanomaterials using the host.

MATERIALS AND METHODS

Materials. All buffers and reagent solutions were prepared using deionized water (H_2O) with resistivity of 18.2 MΩ. Phosphate-buffered saline (PBS), HEPES, tris-borate EDTA buffer (TBE) 10× solutions, and sodium azide reagent were obtained from Bio Basic Canada Inc. (Markham, ON, Canada). PBS buffers were autoclaved prior to use. Gold(III) chloride trihydrate ($HAuCl_4 \cdot 3H_2O$) (99.9% trace metals basis) (gold chloride), sodium citrate tribasic dihydrate (99.0% ACS grade (citrate), hydroquinone (99.5% ReagentPlus) (HQ), sodium chloride (NaCl ACS reagent, > 99.0%), sodium bicarbonate (99.7% ACS grade) (bicarb), agarose (low EEO), Ficoll PM 400, Whatman 0.1 μm nucleopore membrane, hydrogen peroxide (30%) (ACS Reagent), anhydrous chloroform (≥99%), tannic acid, bis(psulfonatophenyl)phenylphosphine dihydrate dipotassium salt (BSPP), BioUltra, ≥98%, sera and albumin from rat, and Millipore Ziptips-C18, glutaraldehyde, sodium nitrite, 5,5′-dithiobis(2-nitrobenzoic acid) (DTNB), formic acid (95−97%), anhydrous acetonitrile (99.8%) (ACN), anhydrous chloroform (≥99%), poly(D,L-lactide-*co*-glycolic acid (PLGA), Triton X-100, sodium cacodylate trihydrate (98%), 2,2′-sulfonyldiethanol solution (TDE), osmium tetraoxide (ACS reagent), and borate buffer were purchased from Sigma-Aldrich (Oakville, ON Canada). Sulfo-cyanine 3-succinimidyl ester (s-Cy3-NHS), sulfo-cyanine 5succinimidyl ester, (s-Cy5-NHS), and sulfo-cyanine 5-maleimide triethylammonium salt (sCy5-Maleimide) was purchased from Click Chemistry Tools, AZ. Methoxy-terminated poly(ethylene glycol) thiol (5 kDa), was obtained from Laysan Bio, Inc. (Arab, AL). 30 kDa and 100kdA Amicon tubes, NuPAGE LDS buffer, NuPAGE MOPS buffer, NuPAGE Novex 4−12% Tris/Bis gel, 20,24-gauge BD PrecisionGlide needles, Alexa Fluor 647 carboxylic acid succinimidyl ester (A647), Sarstedt Microvette CB300 capillary blood collection tube, Fisherbrand disposable borosilicate glass tubes w/plain ends 16 × 150 mm, Illustra NAP-25 columns, and EASY-spray LC columns were purchased from Thermo Fisher Scientific (Burlington, ON, Canada). Whole and heparinized rat blood was recovered from normal healthy female Sprague−Dawley rats from Innovative Research, Novi, MI (cat. no. IR1-150-S). 0.22 μm poly(ether sulfone) syringe (PES) filters, LoBind microcentrifuge tubes (eppendorf tubes), TWEEN-20 (T20), formaldehyde, acrylamide, heparin, sodium dodecyl sulfate (SDS), and DL-dithiothreitol (DTT) were purchased from BioShop Canada, Inc. (Burlington, ON, Canada). Reagent-grade nitric acid (HNO_3), sulfuric (H_2SO_4) hydrochloric acid (HCl), elemental gold, and iodine standards (1000 μg/mL in 2% HCl) were obtained from High-Purity Standards (Charleston, SC). Transmission electron

DOI: 10.1021/acsnano.9b02774
ACS Nano 2019, 13, 8023−8034

microscopy copper grid and uranyl acetate (19485) were purchased from Ted Pella (Redding, CA). Fifteen and 50 mL Falcon tubes were purchased from Biomart Co. (Scarborough, ON, Canada). Methoxy poly(ethylene glycol)-*b*-poly(lactic-*co*-glycolic acid) (mPEG-PLGA), 50:50, 5,000:20 000 Da and (poly(L-lactic) acid-amine (PLLA-NH2,) 5000 Da, were purchased from PolySciTech, IN. Unconjugated *Griffonia simplicifolia* Lectin I (GSL I) (cat. no. L-1100) was purchased from Vector Laboratories. VA-044 azoinitiator (VA-044−500G) was purchased from Wako Chemical, Tokyo, Japan.

Synthesis of Gold Nanoparticles. We used the adapted Frens method[36,37] to prepare 15 nm gold nanoparticles (AuNP). Briefly, 100 μL of 10% (w/v) gold chloride solution was added to 99.9 mL of H_2O, boiled under vigorous stirring, and then reacted with 1 mL of 3% (w/v) citrate for 10 min. Once the reaction was complete, AuNP were cooled on ice, and the size and absorbance were measured to verify quality and concentration (see below). The 15 nm AuNP were also used as seeds for 35, 50, and 80 nm AuNP synthesis.[37] To make 35, 50, and 80 nm AuNP, we sequentially added 86.05 mL (35 nm AuNP), 93.75 mL (50 nm AuNP), and 96.42 mL (80 nm AuNP) of H_2O, 887 μL (35 nm AuNP), 967 μL (50 nm AuNP), and 994 μL (80 nm AuNP) of 25 mM gold chloride, 15 mM citrate, and 11.29 mL (35 nm AuNP), 3.35 mL (50 nm AuNP), and 0.595 mL (80 nm AuNP) of 2.4 nM 15 nm AuNPs to respective Erlenmeyer flasks under vigorous stirring. Next, 887 μL (35 nm AuNP), 967 μL (50 nm AuNP), and 994 μL (80 nm AuNP) of 25 mM HQ were added to the solutions and allowed to stir overnight to complete the reaction. AuNPs solutions were concentrated in 50 mL falcon tubes by centrifugation (3500*g*, 1800*g*, and 1200*g* for 2 hours for 35, 50, and 80 nm AuNPs, respectively). The AuNP pellets were resolubilized in 0.02% (w/v) sodium citrate solution and stored in the dark at 4 °C until further use.

Sub-10 nm Gold Nanoparticle Synthesis. The 8.5 nm AuNP were synthesized according to a different reduction method as developed previously.[38] Briefly, 50 μL of 98.4 mg/mL $HAuCl_4$ was added to 40.2 mL of H_2O in a 250 mL Erlenmeyer flask and stirred at 60 °C for 50 min. Simultaneously, two reducing solutions of 500 μL of 60 mg/mL citrate and 12.5 mg/mL of tannic acid were warmed at 60 °C for 50 min. The first solution was stirred vigorously, and then the second solution was rapidly added. The solution was heated at the same temperature for 30 min and then increased to 100 °C for 10 min. The nanoparticles were added to an ice bath and then cooled to room temperature. One milliliter of 80 mg/mL BSPP was added, and then the mixture was stirred overnight at room temperature. These nanoparticles were washed by centrifugation at 25000*g*.

PEGylation. AuNPs were conjugated with polyethylene glycol (PEG) using thiol-Au coupling chemistry.[1] Briefly, 5K mPEG-SH was dissolved in H_2O at 10 mg/mL. High density PEGylated AuNPs (HP) were prepared by mixing PEG solution with AuNPs at a ratio of 5 PEG/nm^2. The reaction was completed in Eppendorf tubes at 60 °C for 1 hour. Unreacted and excess PEG was removed from these reactions through three rounds of centrifugation (25000*g*, 15000*g*, 3000*g*, 1800*g*, 1000*g*, and 5000*g* for 8, 15, 35, 50, and 80 nm) with PBS. The surface modified PEGylated AuNPs were stored in the dark at 4 °C until injection. The amount of PEG on each AuNP was quantified using a DTNB assay according to manufacturer's instructions. AuNP were also made to clear quickly for the last neural network that confirmed PLGA clearance. These AuNP were incubated at a ratio of 0.5 PEG/nm^2.

Gold Nanoparticle Characterization. Standard characterization techniques such as transmission electron microscopy (TEM), dynamic light scattering (DLS), zeta potential, agarose gel electrophoresis, and ultraviolet−visible spectroscopy (UV−vis) were used to characterize AuNPs.[1] Hydrodynamic size and zeta potential were measured using a Malvern Nano ZS Zetasizer (Malvern Instruments Ltd., Malvern, U.K.). Zeta potential and DLS measurements were done in 10 mM HEPES and 1 mM NaCl. The hydrodynamic size was correlated by measuring the size of the gold core of AuNPs on TEM grids using Hitachi H-7000 transmission electron microscope at an operating voltage between 50 and 100 kV. To visualize the PEG and corona on the nanoparticle surface, the samples were negative stained with 3 μL of 1% uranyl acetate, blotted, and then dried for 1 hour. The mean size and distribution were calculated using ImageJ software (National Institutes of Health, Bethesda, MD). The size-dependent absorbance spectra of AuNPs allowed measurement of concentration as performed previously using UV−vis.

Animals. The 5−6 week-old Sprague−Dawley Rats were purchased from Charles River (Canada). These animals were housed at University of Toronto Division of Comparative Medicine facilities and fed on chow diet.

Nanoparticle Injection and Blood Isolation. All rats were heated for 30 min prior to injection in order to dilate their tail vein to improve the ease of administration. The injected surface area was kept constant for all formulations. All AuNP were administered with a total surface area of 6.28×10^{17}/nm^2. Each injection was diluted to 500 μL. We monitored AuNP in circulation for 24 hours. At each time point, approximately 150−200 μL was collected from saphenous veins using capillary tubes. For the final time point, the rats were sacrificed, and the blood was collected *via* cardiac puncture. Blood was centrifuged at 500*g* for 5 min to separate the serum from cellular debris. For the AuNP samples, the sera appeared pink. The AuNP protein corona was processed using an adapted version previously described by Walkey *et al.*[7] Briefly, 1 mL of PBST (PBS supplemented with 0.05% T20) was added to the NPs and passed through a PES filter to remove any remaining cellular debris. This mixture was then centrifuged for 35 min at 4 °C depending on nanoparticle size and density (25000*g*, 15000*g*, 3000*g*, 1800*g*, and 1000*g* for 8, 15, 35, 50, and 80 nm AuNPs. Supernatant containing unbound proteins was removed and protein coated AuNP pellets were dispersed in 1 mL of PBST followed by another wash with 1 mL of PBS. The subsequent protein coated AuNP pellets were dispersed and divided into aliquots for DLS, zeta potential, and UV−vis and Liquid Chromatography Tandem Mass Spectrometry (LC−MS/MS).

Elemental Analysis of Organs and Blood Using Inductive Coupled-Plasma Mass Spectrometry (ICP−MS). ICP−MS from (NexION; PerkinElmer, Waltham, MA) was used to measure the gold content in the blood and organs from rats following circulation.[13] Borosilicate glass tubes were preweighed prior to blood and organ collection. A water bath was heated to 70 °C, and 400 μL and 1.5 mL of HNO_3 spiked with 1 μg/mL yttrium was added to the blood and organ samples, respectively. The next morning, 144 and 540 μL of HCl was added to the respective samples and digested for 3 hours at 180 °C. The tubes were rinsed with H_2O and diluted to a final volume of 0.5% w/v HCl in 50 mL falcon tubes. Particulates were filtered using a PES filter. A gold standard was prepared to convert counts per seconds to known concentrations.

Bulk Measurement of AlexaFluor 647 Conjugation on Ensemble of Protein Adsorbed AuNPs. A 10 cm^2 (1.27×10^{11} NPs) sample of 50 nm citrate-coated AuNPs was washed with 0.02% w/v citrate and resuspended to a final volume of 100 μL. This aliquot was then added to a solution containing 10 mg/mL of rat serum albumin (RSA) in deionized water or rat serum that was previously filtered through a 0.22 μm filter and incubated at 37 °C for 1 hour. The particles were then centrifuged at 1500−1800*g* for 35 min and washed twice with 0.1 M sodium bicarbonate containing 0.05% (v/v) Tween 20. The particles were then suspended in 100 μL of 0.1 M sodium bicarbonate and mixed with a 5 μg of A647 *N*-hydroxysuccinimidyl ester overnight. The particle aliquots were washed twice in 0.1 M sodium bicarbonate containing 0.05% (v/v) Tween 20 and once with 0.1 M sodium bicarbonate. Purified samples were suspended in 0.1 M sodium bicarbonate and measured using a Tecan Infinite 200 Pro plate reader at an excitation of 640 nm collecting emission at 670 nm. To quantify the number of dyes on each particle, even for those isolated from the animal, a standard calibration curve of AlexaFluor 647 was prepared in 0.1 M bicarbonate.

Single Molecule Fluorescence Imaging of Protein-Coated Gold Nanoparticles. After 50 nm AuNP was purified from the blood, it were diluted in 0.1 M bicarb (pH 8.5), reacted with 10000-fold excess A647, and reacted overnight at room temperature in the dark. The solutions were centrifuged at 1800*g* and washed in 0.1 M

DOI: 10.1021/acsnano.9b02774
ACS Nano 2019, 13, 8023−8034

bicarbT20. A 50 nm citrate stabilized AuNP solution was exposed to a 1 mg/mL solution of RSA dissolved in PBS and incubated at 37 °C for 1 hour. RSA-gold nanoparticles were purified from serum and fluorescently conjugated as described above. The fluorescence among AuNP was retrieved from circulation, AuNP incubated with blood *in vitro*, and RSA-coated AuNP. We etched 25 × 25 mm glass coverslips in piranha solution (2:1, concentrated H_2SO_4/hydrogen peroxide) for 15 min and rinsed them multiple times with H_2O, twice with methanol, and twice with DCM and stored under vacuum until further use.[39] A 100 μL droplet of A647-gold nanoparticles was dispensed in the middle of the etched coverslip, and a second coverslip was placed on top to sandwich the AuNP in place and evenly distribute the solution. Coverslips were imaged using Nikon A1 Confocal Microscope (Apo 60× oil immersion NA 1.40, WD 0.14 mm).

LC−MS/MS Preparation and Analysis. To prepare samples for LC−MS/MS, the PC-AUNP pellets obtained after purification were incubated with 8 μL of 4× LDS buffer and 4 μL of 500 mM DTT at 70 °C to strip off the proteins from AuNP surface.[5] The solution was centrifuged at 18000× for 15 min at 4 °C to pellet aggregated AuNP. The supernatant was isolated to obtain the protein corona. This was added to 950 μL of 10% TCA (w/v) in acetone and incubated overnight at −80 °C to precipitate proteins. The solution was centrifuged at 18000*g* for 15 min at 4 °C to pellet proteins. The supernatant was discarded, and the pellet was resuspended in 500 μL of 0.03% (w/v) aqueous DCA solution and vortexed. A 100 μL portion of 72% (w/v) aqueous TCA solution was added to this, and the solution was chilled on ice for 30 min to precipitate proteins. The solution was centrifuged at 18000*g* for 15 min at 4 °C to pellet proteins. The supernatant was discarded, and the pellet was resuspended in 950 μL of acetone (stored at −30 °C). The solution was incubated for 1 hour at −80 °C to precipitate proteins, which was followed by centrifugation at 18000*g* for 15 min at 4 °C to pellet proteins. The supernatant was discarded and residual acetone was air-dried. The next step for these proteins is trypsin digestion.

Characterization of Protein Corona Using LC MS/MS. Trypsin-digested peptides were analyzed on a linear ion trap-Orbitrap hybrid analyzer (LTQ-Orbitrap Elite hybrid mass spectrometer, ThermoFisher, San Jose, CA) outfitted with a nanospray source and EASY-nLC split-free nano-LC system (ThermoFisher). Samples were first desalted using ZipTips according to the manufacturer's instructions. ZipTips have a maximum loading capacity of 5 μg of analyte, which allowed us to ensure the same amount of protein was analyzed per run. Lyophilized peptide mixtures were dissolved in 0.1% formic acid and loaded onto a 75 μm × 2 cm PepMap 100 Easy-Spray precolumn filled with 3 μm C18 beads followed by an in-line 75 μm × 50 cm PepMax RSLC EASY-Spray analyted column filled with 2 μm C18 beads at a pressure of 600 BAR. Peptides were eluted over 60 min at a rate of 250 nl·min^{-1} using a 0 to 35% ACN gradient in 0.1% formic acid. Peptides were introduced by nanoelectrospray into the LC−MS. The instrument method consisted of one MS full scan (400−1500 m/z) in the Orbitrap mass analyzer, an automatic gain control target of 1×10^6 with a maximum ion injection of 120 ms, one microscan, and a resolution of 240000. Ten data-dependent MS/MS scans were performed in the linear ion trap using the 10 most intense ions at 35% normalized collision energy. The MS and MS/MS scans were obtained in parallel fashion. In MS/MS mode, automatic gain control targets were 1×10^5 with a maximum ion injection time of 50 ms. A minimum ion intensity of 5000 was required to trigger an MS/MS spectrum. Normalized collision energy was set to 35. Dynamic exclusion was applied using a maximum exclusion list of 500 with one repeat count of duration 30 s and an exclusion duration of 15 s.

Proteomics-Statistics Analysis. We converted extracted ion currents to label-free quantitative (LFQ) intensities according to the standard publication (version 8.6, Bioinformatics Solutions Inc. Waterloo, ON, Canada).[8,26,27] These LFQ intensities were either processed in GraphPad Prism v6.01 or JMP Pro statistical discovery software (V12.2.0) from SAS Institute Inc. to generate heat maps, hierarchical cluster, principal component analyses and to build the neural network. The Multivariate Methods platform in JMP was used for hierarchical clustering (Ward method), and Principal Component Analysis. When comparing the coefficients of variance and their significant or nonsignificant differences, we are referring to the F score. The F score tells us whether the variance we see is based on chance. When the F score is greater than the critical F value (P value < α (0.025), we reject the null hypothesis and then confirm whether the differences in protein profile are significantly different.

Neural Network. We had a total of 18 rats across five conditions with five different time points. Time points were treated as five independent data points per biological replicate. Our mass spectrometry analysis discovered 707 significant proteins. Therefore, the neural network was trained on 63630 protein LFQ intensities. The output data for building the network was acquired through quantification of blood half-life and liver and spleen uptake by measuring gold using ICP−MS. The diameter was determined using TEM. We next developed and trained a neural network with two hidden layers and three nodes per layer using the JMP Pro Software Suite.[29] The first node is a nonlinear activation function and the second node a linear activation function. The weighting from the first node to the second changes through multiple rounds of feedforward and backpropagation learning to yield the final network that can predict the desired output parameters. We transformed the data with a two-layer hyperbolic tangent function for 375 epochs with a squared penalty function. Weights were automatically optimized using gradient boosting. We regularized the network to avoid overfitting by using early stopping and K-fold cross validation. The JMP neural network optimization algorithm employs a cross validation based early stopping rule that proceeds until the average test error reached a minimum. To also help ensure we did not overfit the data, we applied a K-fold validation method with five-folds. Overall, we ensured overfitting was not an issue by our use of blind test data never seen by the classifier. The size of the test set was 21210 data input points. This was derived from 30 samples. These 30 samples are derived from 2 nanoparticles × 3 replicates × 5 time points × 707 proteins. We then input the proteomic values from the two unknown sizes and ran the neural network model. The outputs were recorded as single values and plotted using GraphPad Prism.

Sparse Feature Selection. In order to determine what proteins have the greatest effect on predicting biological behavior, we employed a sparse feature selection prior to training another neural network. Sparse feature selection simplifies the data set by reducing the redundancy of the data set. Performing these methods are valuable because they help to obtain a subset of predictors that minimize error for the quantitative response variable. This way, we can examine what proteins are the best predictors of nanoparticle biological fate. There are a variety of ways to do this so we tried a different models such as ridge regression, elastic nets lasso, double lasso and adaptive lasso. Adaptive lasso produced a subset of proteins that predicted biological behavior with the highest accuracy. Adaptive lasso penalizes the variables and identifies those that have the coefficients that are closest to zero and/or have an actual effect on the response. We used the JMP platform to perform an Adaptive Lasso with K-fold validation for five folds and a minimum penalty fraction of 0.001 to reduce the total number of proteins to 21.[34,35] We retrained the deep neural network by using these 21 proteins as our input variables and still used half-life, and liver and spleen accumulation as outputs. Once we trained the neural network we then tested it on the unknown nanoparticle data set. We used the same 21 proteins for the unknown nanoparticles. After running the neural network, we took the predicted outputs, compared it the real values, calculated its prediction accuracy, and then compared its accuracy to the previous neural network that was trained on all 707.

Serial Injection of Materials for Biological Analysis. In this experiment, we injected 50 nm PEGylated AuNPs into healthy rats (donors) and then isolated them from blood at different times in circulation. Isolated nanoparticles were then reinjected into a new set of healthy rats (acceptors) for investigating the impact of protein adsorption in the donor rat on biodistribution in the acceptor rat. We injected 2×10^{14} AuNPs into each donor rat. An 8−10 mL portion of blood was isolated from each rat at a specific time (1, 2, 8, or 24

DOI: 10.1021/acsnano.9b02774
ACS Nano 2019, 13, 8023−8034

hours) post injection, and nanoparticles were isolated from blood using the same procedure as described above. These nanoparticles had acquired proteins from blood at the time of isolation. We then injected 2×10^{13} AuNPs into acceptor rats and allowed them to circulate for 24 hours. After 24 hours, rats were sacrificed, and liver and spleen were digested and processed for measuring nanoparticle accumulation using ICP−MS as described above. We also injected 2×10^{13} AuNPs into healthy rats as control to measure the difference in biodistribution. These are labeled as PEG control in text. For 3D Imaging and TEM, we repeated this SIMBA procedure and perfused with fixatives as described in the next section.

Transcardial Perfusion Fixation for 3D Imaging. Perfusion procedures used were the same as published previously.[40−42] A 0.6 mL portion of GSL1-Cy3 (1 mg/mL) was injected intravenously *via* the tail vein to label rat vasculature and allowed to circulate for 5 min. Rats were then anaesthetized under continuous flow of 4% (v/v) isoflurane in oxygen. Surgical procedures to access heart were performed by opening ribs and dissecting along the sides. Needle was inserted in the left ventricle and 800 mL of PBS solution which contains 10 U/mL heparin and 0.5% (w/v) sodium nitrite in 1× PBS was injected at a constant flow rate of 60 mL/min. Next, 800 mL of monomer solution was infused at the same flow rate. This monomer solution is made of 4% formaldehyde, 2% acrylamide, and 0.25% initiator in 1× PBS solution. After perfusion, liver and spleen were resected and incubated in 30 mL of same monomer solution at 4 °C for another 7 days.

Tissue Cross-linking for 3D Imaging. After 1 week of incubation with monomer solution, the tissues were cross-linked as described elsewhere.[40−42] The monomer solution was replaced with 30 mL of the same freshly prepared solution. The samples were degassed and purged with argon 3 times. During these cycles, the caps on the falcon tubes were perforated. This removed most of the oxygen and the tubes were sealed by tightening caps and sealing with parafilm. The samples were polymerized at 37 °C with shaking for 3 hours. The solution was viscous due to cross-linking at the end of this cycle. Excess solution was removed, and gelled tissues were rinsed with deionized water and then stored in 10 mL of borate buffer (200 mM sodium borate, pH 8.5, 0.1% Triton-X100 and 0.01% sodium azide) at 4 °C.

Tissue Clearing and Imaging. Tissues were cleared passively as established previously.[40−42] After gelling in the previous step, tissues were placed in the clearing solution (4% (w/v) SDS and 200 mM sodium borate at pH 8.5) for 2 weeks at 50 °C using 15 mL of clearing solution for 1−2 mm slices. Once cleared, these were stored at 4 °C in borate buffer. For imaging, tissues were immersed in 67% TDE solution and imaged with light sheet microscopy as described in previously published work.[40−42]

Sample Preparation for Transmission Electron Microscopy. Samples for electron microscopy were prepared by Doug Holmyard at Nanoscale Biomedical Imaging facility at SickKids Hospital. Monomer perfused fixed samples were transferred to a solution of 4% formaldehyde and 0.5% (w/v) glutaraldehyde in 1× PBS. The facility then fixed the tumor in in 2% (w/v) glutaraldehyde in 0.1 M sodium cacodylate buffer, rinsed with buffer, postfixed in 1% osmium tetroxide in buffer, dehydrated in a graded ethanol series followed by propylene oxide, and embedded in Quetoi-Spurr resin. Next, sections with a thickness of 90 nm were cut on a Leica Ultracut ultramicrotome, stained with uranyl acetate and lead citrate and digitally imaged using a FEI Tecnai 20 Transmission electron microscope.

Synthesis of mPEG−PLGA/PLGA/PLLA-Cy5 Nanoparticles. PLLA was first conjugated with Cy5 in dimethylformamide and then lyophilized to obtain the final solid PLLA-Cy5. Two mg of mPEG−PLGA and 8 mg of PLLA-Cy5 were reacted in 1 mL of acetonitrile. The polymer mixture solution was then added dropwise into 5 mL of rapidly stirring water and allowed to react overnight.[5] PLGA nanoparticles were purified with 100 kDa centrifugal filters and then characterized using DLS, TEM, and fluorescence spectroscopy.[43] We confirmed that no free protein remained after purification using polyacrylamide gel electrophoresis (PAGE). After running the PAGE according to manufacturers instructions, we imaged it on a Carestream Multispectral MS Fx Pro *in vivo* imager (excitation/emission: 750/830 nm) with a 10 min exposure time.

PLGA Injection and Blood Isolation. All methods and nanoparticle numbers remained the same except PLGA was injected and collected every 15 min for 90 min.

Statistics. All statistics were performed using GraphPad Prism v6.01, and JMP Pro statistical discovery software, V12.2.0, from SAS Institute, Inc., Cary, NC, 1989−2018.

ASSOCIATED CONTENT

Supporting Information

The Supporting Information is available free of charge on the ACS Publications website at DOI: 10.1021/acsnano.9b02774.

Python codes and protein information (ZIP)
Bare PEGylated AuNP control (MP4)
1 h donor nanoparticles (MP4)
2 h donor nanoparticles (MP4)
8 h donor nanoparticles (MP4)
24 h donor nanoparticles (MP4)
Supporting figures (PDF)

AUTHOR INFORMATION

Corresponding Author

*E-mail: warren.chan@utoronto.ca.

ORCID

Warren C. W. Chan: 0000-0001-5435-4785

Author Contributions

[∇]J.L., S.S., and A.J.T. contributed equally to this work. J.L., A.J.T., S.S. and W.C.W.C. conceived the idea and wrote the manuscript. All authors analyzed the data. M.B.P. performed the single molecule analysis. All authors read and commented on the manuscript.

Notes

The authors declare no competing financial interest.
The neural networks built for testing performance will be made available upon request

ACKNOWLEDGMENTS

We thank Maxim B. Prigozhin from Stanford University for his support with the single molecule fluorescence analysis. We thank Canadian Institutes of Health Research (FDN-159932, MOP-1301431), NSERC (2015-06397), Collaborative Health Research Program (CPG-146468), Canadian 464 Research Chairs Program (950-223824), and the Canadian Cancer Society (705285-1) for funding support.

REFERENCES

(1) Walkey, C. D.; Olsen, J. B.; Guo, H.; Emili, A.; Chan, W. C. W. Nanoparticle Size and Surface Chemistry Determine Serum Protein Adsorption and Macrophage Uptake. *J. Am. Chem. Soc.* **2012**, *134*, 2139−2147.

(2) Walkey, C. D.; Chan, W. C. W. Understanding and Controlling the Interaction of Nanomaterials with Proteins in a Physiological Environment. *Chem. Soc. Rev.* **2012**, *41*, 2780−2799.

(3) Bertrand, N.; Grenier, P.; Mahmoudi, M.; Lima, E. M.; Appel, E. A.; Dormont, F.; Lim, J. M.; Karnik, R.; Langer, R.; Farokhzad, O. C. Mechanistic Understanding of *in Vivo* Protein Corona Formation on Polymeric Nanoparticles and Impact on Pharmacokinetics. *Nat. Commun.* **2017**, *8*, 777.

(4) Tenzer, S.; Docter, D.; Kuharev, J.; Musyanovych, A.; Fetz, V.; Hecht, R.; Schlenk, F.; Fischer, D.; Kiouptsi, K.; Reinhardt, C.; Landfester, K.; Hansjörg, S.; Maskos, M.; Knauer, S. K.; Stauber, R. H.

DOI: 10.1021/acsnano.9b02774
ACS Nano 2019, 13, 8023−8034

Rapid Formation of Plasma Protein Corona Critically Affects Nanoparticle Pathophysiology. *Nat. Nanotechnol.* **2013**, *8*, 772−781.
(5) Lundqvist, M.; Stigler, J.; Cedervall, T.; Berggård, T.; Flanagan, M. B.; Lynch, I.; Elia, G.; Dawson, K. The Evolution of the Protein Corona around Nanoparticles: A Test Study. *ACS Nano* **2011**, *5*, 7503−7509.
(6) Lundqvist, M.; Stigler, J.; Elia, G.; Lynch, I.; Cedervall, T.; Dawson, K. A. Nanoparticle Size and Surface Properties Determine the Protein Corona with Possible Implications for Biological Impacts. *Proc. Natl. Acad. Sci. U. S. A.* **2008**, *105*, 14265−14270.
(7) Walkey, C. D.; Olsen, J. B.; Song, F.; Liu, R.; Guo, H.; Olsen, W.; Cohen, Y.; Emili, A.; Chan, W. C. W. Protein Corona Fingerprinting Predicts the Cell Association of Gold Nanoparticles. *ACS Nano* **2014**, *8*, 2439−2455.
(8) Chen, F.; Wang, G.; Griffin, J. I.; Brenneman, B.; Banda, N. K.; Holers, V. M.; Backos, D. S.; Wu, L.; Moghimi, S. M.; Simberg, D. Complement Proteins Bind to Nanoparticle Protein Corona and Undergo Dynamic Exchange *in Vivo*. *Nat. Nanotechnol.* **2017**, *12*, 387−393.
(9) Hadjidemetriou, M.; Al-Ahmady, Z.; Mazza, M.; Collins, R. F.; Dawson, K.; Kostarelos, K. *In Vivo* Biomolecule Corona around Blood-Circulating, Clinically Used and Antibody-Targeted Lipid Bilayer Nanoscale Vesicles. *ACS Nano* **2015**, *9*, 8142−8156.
(10) Xu, M.; Soliman, M. G.; Sun, X.; Pelaz, B.; Feliu, N.; Parak, W. J.; Liu, S. How Entanglement of Different Physicochemical Properties Complicates the Prediction of *in Vitro* and *in Vivo* Interactions of Gold Nanoparticles. *ACS Nano* **2018**, *12*, 10104−10113.
(11) Feliu, N.; Docter, D.; Heine, M.; Del Pino, P.; Ashraf, S.; Kolosnjaj-Tabi, J.; Macchiarini, P.; Nielsen, P.; Alloyeau, D.; Gazeau, F.; Stauber, R. H.; Parak, W. J. *In Vivo* Degeneration and the Fate of Inorganic Nanoparticles. *Chem. Soc. Rev.* **2016**, *45*, 2440−2457.
(12) Setyawati, M. I.; Tay, C. Y.; Docter, D.; Stauber, R. H.; Leong, D. T. Understanding and Exploiting Nanoparticles' Intimacy with the Blood Vessel and Blood. *Chem. Soc. Rev.* **2015**, *44*, 8174−8199.
(13) Sykes, E. A.; Dai, Q.; Tsoi, K. M.; Hwang, D. M.; Chan, W. C. W. Nanoparticle Exposure in Animals Can Be Visualized in the Skin and Analysed *via* Skin Biopsy. *Nat. Commun.* **2014**, *5*, 3796−3803.
(14) Perry, J.; Reuter, K.; Kai, M.; Herlihy, K. PEGylated PRINT Nanoparticles: The Impact of PEG Density on Protein Binding, Macrophage Association, Biodistribution, and Pharmacokinetics. *Nano Lett.* **2012**, *12*, 5304−5310.
(15) Angermueller, C.; Pärnamaa, T.; Parts, L.; Stegle, O. Deep Learning for Computational Biology. *Mol. Syst. Biol.* **2016**, *12*, 878.
(16) Tarca, A. L.; Carey, V. J.; Chen, X.-w.; Romero, R.; Drăghici, S. Machine Learning and Its Applications to Biology. *PLoS Comput. Biol.* **2007**, *3*, 953−962.
(17) Hastie, T.; Tibshirani, R.; Friedman, J. The Elements of Statistical Learning. *Math. Intell.* **2001**, *27* (2), 83−85.
(18) Jokerst, J. V.; Lobovkina, T.; Zare, R. N.; Gambhir, S. S. Nanoparticle PEGylation for Imaging and Therapy. *Nanomedicine* **2011**, *6*, 715−728.
(19) Shah, N. B.; Vercellotti, G. M.; White, J. G.; Fegan, A.; Wagner, C. R.; Bischof, J. C. Blood-Nanoparticle Interactions and *in Vivo* Biodistribution: Impact of Surface PEG and Ligand Properties. *Mol. Pharmaceutics* **2012**, *9*, 2146−2155.
(20) Niidome, T.; Yamagata, M.; Okamoto, Y.; Akiyama, Y.; Takahashi, H.; Kawano, T.; Katayama, Y.; Niidome, Y. PEG-Modified Gold Nanorods with a Stealth Character for *in Vivo* Applications. *J. Controlled Release* **2006**, *114*, 343−347.
(21) Xie, J.; Xu, C.; Kohler, N.; Hou, Y.; Sun, S. Controlled PEGylation of Monodisperse Fe3O4 Nanoparticles for Reduced Non-Specific Uptake by Macrophage Cells. *Adv. Mater.* **2007**, *19*, 3163−3166.
(22) Dai, Q.; Walkey, C.; Chan, W. C. W. Polyethylene Glycol Backfilling Mitigates the Negative Impact of the Protein Corona on Nanoparticle Cell Targeting. *Angew. Chem., Int. Ed. Engl.* **2014**, *53*, 5093−5096.
(23) Rausch, K.; Reuter, A.; Fischer, K.; Schmidt, M. Evaluation of Nanoparticle Aggregation in Human Blood Serum. *Biomacromolecules* **2010**, *11*, 2836−2839.
(24) Albanese, A.; Chan, W. Effect of Gold Nanoparticle Aggregation on Cell Uptake and Toxicity. *ACS Nano* **2011**, *5*, 5478−5489.
(25) Grossmann, J.; Roschitzki, B.; Panse, C.; Fortes, C.; Barkow-Oesterreicher, S.; Rutishauser, D.; Schlapbach, R. Implementation and Evaluation of Relative and Absolute Quantification in Shotgun Proteomics with Label-Free Methods. *J. Proteomics* **2010**, *73*, 1740−1746.
(26) Cox, J.; Hein, M. Y.; Luber, C. A.; Paron, I.; Nagaraj, N.; Mann, M. Accurate Proteome-Wide Label-Free Quantification by Delayed Normalization and Maximal Peptide Ratio Extraction, Termed MaxLFQ. *Mol. Cell. Proteomics* **2014**, *13*, 2513−2526.
(27) Zhang, J.; Xin, L.; Shan, B.; Chen, W.; Xie, M.; Yuen, D.; Zhang, W.; Zhang, Z.; Lajoie, G. A.; Ma, B. PEAKS DB: *De Novo* Sequencing Assisted Database Search for Sensitive and Accurate Peptide Identification. *Mol. Cell. Proteomics* **2012**, *11*, M111.010587.
(28) Albanese, A.; Tang, P. S.; Chan, W. C. W. The Effect of Nanoparticle Size, Shape, and Surface Chemistry on Biological Systems. *Annu. Rev. Biomed. Eng.* **2012**, *14*, 1−16.
(29) Gotwalt, C. M. *JMP Neural Network Methodology* **2012**, 1−11.
(30) Li, Y. P.; Pei, Y. Y.; Zhang, X. Y.; Gu, Z. H.; Zhou, Z. H.; Yuan, W. F.; Zhou, J. J.; Zhu, J. H.; Gao, X. J. PEGylated PLGA Nanoparticles as Protein Carriers: Synthesis, Preparation and Biodistribution in Rats. *J. Controlled Release* **2001**, *71*, 203−211.
(31) Campbell, F.; Bos, F. L.; Sieber, S.; Arias-alpizar, G.; Kros, A.; Bussmann, J. Directing Nanoparticle Biodistribution through Directing Nanoparticle Biodistribution through Evasion and Exploitation of Stab2-Dependent Nanoparticle Uptake. *ACS Nano* **2018**, *12*, 2138−2150.
(32) Qie, Y.; Yuan, H.; von Roemeling, C. A.; Chen, Y.; Liu, X.; Shih, K. D.; Knight, J. A.; Tun, H. W.; Wharen, R. E.; Jiang, W.; Kim, B. Y. S. Surface Modification of Nanoparticles Enables Selective Evasion of Phagocytic Clearance by Distinct Macrophage Phenotypes. *Sci. Rep.* **2016**, *6*, 1−10.
(33) Schöttler, S.; Becker, G.; Winzen, S.; Steinbach, T.; Mohr, K.; Landfester, K.; Mailänder, V.; Wurm, F. R. Protein Adsorption Is Required for Stealth Effect of Poly(Ethylene Glycol)- and Poly-(Phosphoester)- Coated Nanocarriers. *Nat. Nanotechnol.* **2016**, *11*, 372−377.
(34) Autefage, H.; Gentleman, E.; Littmann, E.; Hedegaard, M. A. B.; Von Erlach, T.; O'Donnell, M.; Burden, F. R.; Winkler, D. A.; Stevens, M. M. Sparse Feature Selection Methods Identify Unexpected Global Cellular Response to Strontium-Containing Materials. *Proc. Natl. Acad. Sci. U. S. A.* **2015**, *112*, 4280−4285.
(35) Figueiredo, M. A. T. Adaptive Sparseness for Supervised Learning. *IEEE Trans. Pattern Anal. Mach. Intell.* **2003**, *25*, 1150−1159.
(36) Frens, G. Controlled Nucleation for the Regulation of the Particle Size in Monodisperse Gold Suspensions. *Nature, Phys. Sci.* **1973**, *241*, 20−22.
(37) Perrault, S. D.; Chan, W. C. W. Synthesis and Surface Modification of Highly Monodispersed, Spherical Gold Nanoparticles of 50−200 Nm. *J. Am. Chem. Soc.* **2009**, *131*, 17042−17043.
(38) Chou, L. Y. T.; Zagorovsky, K.; Chan, W. C. W. DNA Assembly of Nanoparticle Superstructures for Controlled Biological Delivery and Elimination. *Nat. Nanotechnol.* **2014**, *9*, 148−155.
(39) Engle, K. M.; Mei, T.-S.; Wasa, M.; Yu, J.-Q. Semiconductor Quantum Rods as Single Molecule Fluorescent Biological Labels. *Acc. Chem. Res.* **2008**, *45*, 788−802.
(40) Syed, A. M.; Sindhwani, S.; Wilhelm, S.; Kingston, B. R.; Lee, D. S. W.; Gommerman, J. L.; Chan, W. C. W. Three-Dimensional Imaging of Transparent Tissues *via* Metal Nanoparticle Labeling. *J. Am. Chem. Soc.* **2017**, *139*, 9961−9971.
(41) Sindhwani, S.; Syed, A. M.; Wilhelm, S.; Chan, W. C. W. Exploring Passive Clearing for 3d Optical Imaging of Nanoparticles in Intact Tissues. *Bioconjugate Chem.* **2017**, *28*, 253−259.

DOI: 10.1021/acsnano.9b02774
ACS Nano 2019, 13, 8023−8034

(42) Sindhwani, S.; Syed, A. M.; Wilhelm, S.; Glancy, D. R.; Chen, Y. Y.; Dobosz, M.; Chan, W. C. W. Three-Dimensional Optical Mapping of Nanoparticle Distribution in Intact Tissues. *ACS Nano* **2016**, *10*, 5468−5478.
(43) Panagi, Z.; Beletsi, A.; Evangelatos, G.; Livaniou, E.; Ithakissios, D. S.; Avgoustakis, K. Effect of Dose on the Biodistribution and Pharmacokinetics of PLGA and PLGA-MPEG Nanoparticles. *Int. J. Pharm.* **2001**, *221*, 143−152.

DOI: 10.1021/acsnano.9b02774
ACS Nano 2019, 13, 8023−8034